Identification of ocular dominance domains in New World owl monkeys by immediate-early gene expression

Toru Takahata[a], Masanobu Miyashita[b], Shigeru Tanaka[c], and Jon H. Kaas[a,1]

[a]Department of Psychology, Vanderbilt University, Nashville, TN 37240; [b]Division of Control and Computer Engineering, Numazu National College of Technology, Numazu, Shizuoka 410-8501, Japan; and [c]Brain Science Inspired Life Support Research Center, The University of Electro-Communications, Chofu, Tokyo 182-8585, Japan

Ocular dominance columns (ODCs) have been well studied in the striate cortex (V1) of macaques, as well defined arrays of columnar structure that receive inputs from one eye or the other, whereas ODC expression seems more obscure in some New World primate species. ODCs have been identified by means of eye injections of transneuronal transporters and examination of cytochrome oxidase (CO) activity patterns after monocular enucleation. More recently, live-imaging techniques have been used to reveal ODCs. Here, we used the expression of immediate-early genes (IEGs), protooncogene, *c-Fos*, and zinc finger protein, *Zif268*, after monocular inactivation (MI) to identify ODCs in V1 of New World owl monkeys. Because IEG expression is more sensitive to activity changes than CO expression, it is capable of revealing activity maps in all layers throughout V1 and demonstrating brief activity changes within a couple of hours. Using IEGs, we not only revealed apparent ODCs in owl monkeys but also discovered a number of unique features of their ODCs. Distinct from those in macaques, these ODCs sometimes bridged to other columns in layer 4 (Brodmann layer 4C). CO blobs straddled ODC borders in the central visual field, whereas they centered ODC patches in the peripheral visual field. In one case, the ODC pattern continued into V2. Finally, an elevation of IEG expression in layer 4 (4C) was observed along ODC borders after only brief MI. Our data provide insights into the structure and variability of ODCs in primates and revive debate over the functions and development of ODCs.

Aotus | border strip | CO puff | stereopsis | tetrodotoxin

Ocular dominance columns (ODCs) were first identified by Hubel and Wiesel in cats and macaques in the 1960s (1). They have been characterized as columnar structures penetrating layers 2–6 of striate cortex (primary visual cortex, area 17, V1) that predominantly receive inputs from either the right or left eye via the lateral geniculate nuclei (LGN). In macaques, histologically identified ODCs constantly form alternating stripes 400–500 μm in width throughout layer 4 (Brodmann area 4C) of V1 except for the monocular segment (MS) created by the optic disk and peripheral monocular visual field (2, 3). Attempts to reveal ODCs in New World monkeys have produced varied and limited results. Even though some of the New World monkeys, cebus and spider monkeys, have ODCs much like those in macaques (4, 5), it seems that many small primate species may not have ODCs, or that the ODCs are variably expressed, raising questions about the functional roles of the ODC (6). Only obscure or no ODCs were revealed in owl monkeys (7–9). Marmosets apparently lose their ODCs during early postnatal development (10). Squirrel monkeys have capricious patterns of ODCs that vary from individual to individual (11). However, these observations have been obtained in studies using traditional techniques to reveal ODCs, such as tracer transport studies and cytochrome-oxidase (CO) staining of V1 after monocular enucleation. These methods may not be sensitive enough to reveal ODCs in smaller primates. Indeed, some evidence for the presence of ODCs in adult marmosets

has been more recently obtained (12, 13), and investigations using intrinsic signal-optical imaging have revealed clusters of ocular dominance cells in V1 of owl monkeys and prosimian galagos (14, 15).

In this study, we applied another method to reveal functional compartments related to ocular dominance in V1 of New World owl monkeys. We examined mRNA expression of immediate-early genes (IEGs) protooncogene, *c-Fos*, and zinc finger protein, *Zif268*, after monocular inactivation (MI) produced by injections of the sodium channel blocker TTX into one eye. The expression of IEG is highly dependent on neuronal activity and is even sensitive to activity changes as short as 1 h (16, 17). Another advantage of this method is its capability of revealing ODCs throughout all of the layers over the entire extent of visual cortices, whereas other methods reveal patterns in only a limited portion of V1 or only the patterns in layer 4. In our previous study, the IEG method revealed functional components of ODCs that are normally cryptic to conventional techniques in macaques (16). With this IEG method, we were able to more fully study the unique morphology of ODCs of owl monkeys.

Results

In situ hybridization (ISH) for IEG in an owl monkey that was subjected to MI for 24 h revealed stripes and patches of alternating dense and light signals in V1 (Fig. 1 A and B), whereas CO reaction was uniform throughout V1 (Fig. 1C). Because this IEG pattern was not observed in visually intact owl monkeys, we hypothesize that the pattern represents ODCs, with stronger signals from the activated eye inputs and weaker signals from the inactivated eye inputs. In previous and current studies in owl monkeys, we used Hässler's scheme of the V1 layering (18), where only layer 4C of Brodmann is considered to be layer 4.

Significance

Ocular dominance columns (ODCs), the segregation of activation patterns from each eye in primary visual cortex, are variable in form but are present in most studied primates. However, their existence seems to be weak or absent in nocturnal owl monkeys, raising questions about the significance of ODCs. Using the highly sensitive method of immediate-early genes after monocular deprivation, we revealed an unusual pattern of eye-dependent activity in V1, providing further evidence for the widespread presence and variability of ODCs in primates and raising further questions about their development and functions.

NEUROSCIENCE
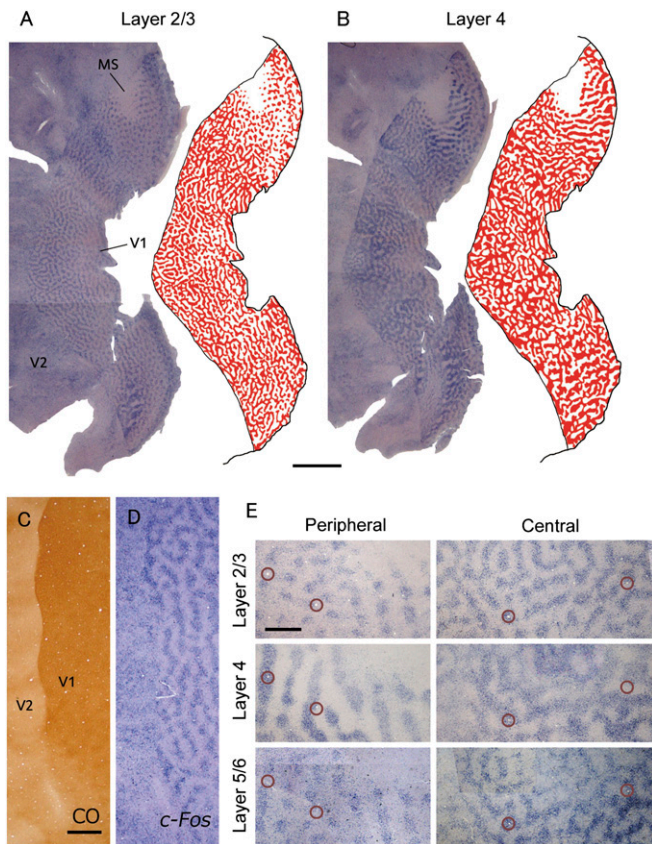
Fig. 1. An owl monkey case (ID 11-04) subjected to MI in the left eye for 24 h. An ODC-like pattern was revealed by IEG expression throughout V1 except in the presumptive MS. (*A* and *B*) Tangential sections of whole flattened V1 contralateral to the inactivated eye reacted for *c-Fos* mRNA (*A*) 640 μm from the pial surface, mostly in layer 3, and (*B*) 880 μm from the pial surface, mostly in layer 4 (4C). ODC-like patterns in layer 2/3 (*A*) and layer 4 (4C) (*B*) were illustrated by red on the right side of the sections. (Scale bar, 5 mm.) (*C* and *D*) Higher magnification of the adjacent tangential sections stained for CO activity (*C*, 720 μm from the pial surface) and *c-Fos* mRNA (*D*, 640 μm) around the V1/V2 border. (Scale bar, 1 mm.) (*E*) Flattened sections stained for *c-Fos* mRNA, showing differences in ODC-like patterns across layers and V1 regions. Circles indicate the same radial blood vessels across layers. Depths are 640 μm (*Top*), 880 μm (*Middle*), and merge of 1,120 μm and 1,240 μm (*Bottom*) of peripheral V1, respectively, and 640 μm (*Top*), merge of 760 μm and 880 μm (*Middle*), and merge of 1,000 μm and 1,040 μm (*Bottom*) of central V1. (Scale bar, 1 mm.)

Here we also use Hässler's terms for layers, and Brodmann's layers and sublayers are noted in parentheses. In layer 4 (4C), the width of the postulated ODCs dramatically varied from 300 to 600 μm, which is different from that in macaques (19). The postulated MS was also observed in the dorsomedial aspect of V1, as a homogeneously weak region of ISH signals contralateral to the inactivated eye (Fig. 1 *A* and *B*) and a homogeneously intense region of signals in the ipsilateral V1 (Fig. S1). A region of low signals for the optic disk of the contralateral eye was not seen, most likely because it locates at the edge of the section. The ODCs were observed as small patches around MS, representing the far peripheral visual field. Although the stripes of ODCs in macaques intersect the V1/V2 border at right angles, such a geometric relationship was not observed in this owl monkey (Fig. 1*D*). Surprisingly, the ODCs were distinct across layers 2–6 in the owl monkey (Fig. 1*E*). ODC patterns were almost identical in the supragranular and infragranular layers. However, the patterns of ODCs in granular layer formed broader stripes or patches than in the infragranular or supragranular layers.
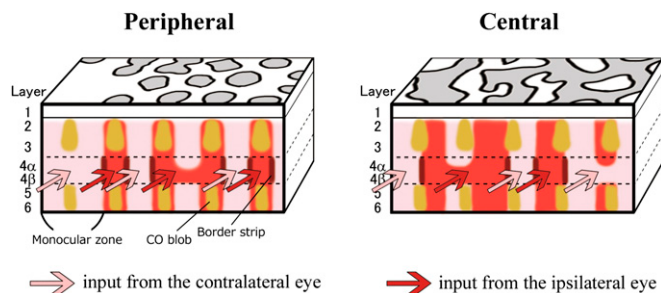
In another owl monkey with 24-h MI (Fig. 2 *A* and *B*) we observed ODC patterns across flattened cortex comparable to those in the first case. Unexpectedly, the ODC stripes extended beyond the V1/V2 border into entire V2 in this case (Fig. 2 *C* and *D*). This extension into V2 was most obvious in the middle cortical layers. When the left hemisphere of this monkey was cut into coronal sections, the columnar patterns observed in V1 also continued into V2 (Fig. 2 *E* and *F*). At higher magnification, distinct patterns of ODC were observed in V1, especially in layer 4β (4Cβ), where OD domains are occasionally much broader than those in other layers (Fig. 2 *G–I*).

To quantitatively compare CO staining and IEG methods, we measured relative optical density (ROD) within layer 4 (4C) in the images of tangential brain section processed for CO or IEG. Those two images from the flattened visual cortex were digitally aligned with the guidance of shared blood vessels across adjacent brain sections (Fig. 3 *A* and *B*). Regions of interest (ROIs) were taken for pale columns (PCs) and dark columns (DCs), representing ODCs for the blocked eye and intact eye, respectively, in the IEG images. Then, the ROI were applied to the adjacent CO
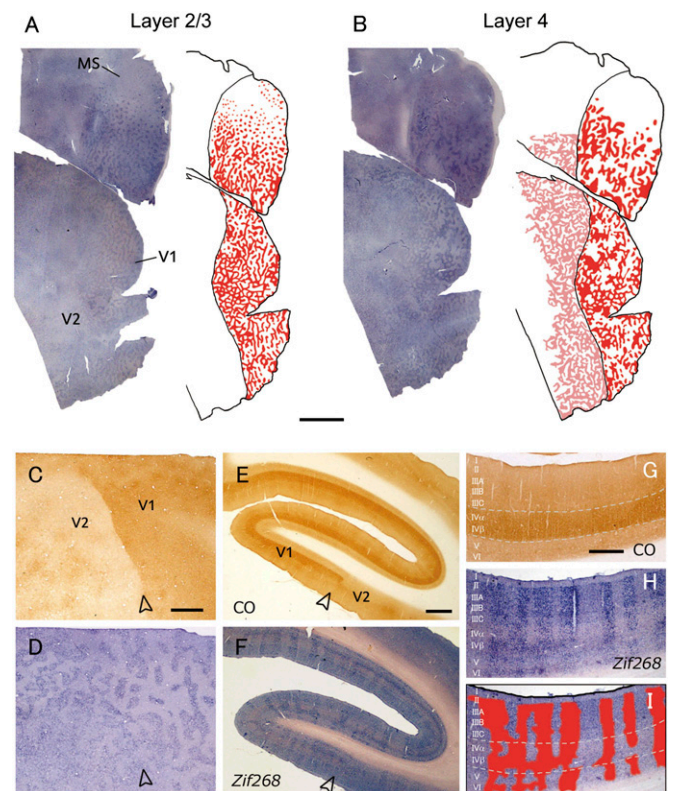
Fig. 2. Another owl monkey case (ID 09-41) subjected to MI in the left eye for 24 h. In this case, an ODC-like pattern was revealed continuously from V1 to V2 by IEG expression. (*A* and *B*) Tangential sections of whole V1 and V2 contralateral to the inactivated eye reacted for *c-Fos* mRNA (*A*) 600 μm from the pial surface, mostly in layer 3 and (*B*) 780 μm from the pial surface, mostly in layer 4 (4C). ODC-like patterns in layer 2/3 (*A*) and layer 4 (4C) (*B*) were illustrated by red on the right of the sections. In addition, ODC-like pattern in layer 4 of V2 was illustrated by pink in *B*. (Scale bar, 5 mm.) (*C* and *D*) Higher magnification of the adjacent tangential sections stained for CO activity (*C*, 900 μm from the pial surface) and *c-Fos* mRNA (*D*, 780 μm) around the V1/V2 border. (Scale bar, 1 mm.) (*E* and *F*) Adjacent coronal sections of ipsilateral V1–V2 to the blocked eye, stained for CO activity (*E*) and *Zif268* mRNA (*F*). (Scale bar, 1 mm.) (*G–I*) Higher magnification of adjacent coronal V1 sections stained for CO (*G*) and *Zif268* mRNA (*H*). ODC-like pattern was illustrated by red in *I* over the image of *H*. Open arrowheads indicate V1/V2 border. (Scale bar, 500 μm.)

Fig. 3. Comparison between IEG mRNA expression and CO staining patterns. (*A* and *B*) The tangential cortical sections of V1 from the monkey subjected to 24-h MI (ID 11-04), stained for *c-Fos* mRNA (*A*) or CO activity (*B*). The depth from the pial surface is 1,000 μm and 960 μm, respectively, representing mostly layer 4 (4C). The two images are aligned exactly at the same V1 portion, guided by the radial blood vessels (brown open circles). L4/layer 4, L5/layer 5. (Scale bar, 1 mm.) (*C*) Quantification of signal intensity of ISH for *c-Fos* and CO activity. ROIs were taken for DCs and PCs from the ISH image as illustrated by white and black dotted lines in *A*, respectively, and also applied to the CO staining image. RODs of PC were significantly lower than those of DC in ISH images (**$P < 0.01$, paired Student *t* test, six sections), whereas they were not in CO staining images ($P = 0.19$).

image. Data were taken from six sections of three cortices of two animals (ID 11-04 and 09-41). Whereas the IEG pattern showed a significant difference in ROD between ROIs in PCs and DCs ($P < 0.01$), RODs of CO staining in PCs were almost identical to those in DCs ($P = 0.19$) (Fig. 3*C*). Thus, MI treatment reduced the IEG expression in deprived domains in cortex whereas CO activity was unchanged.

No alignments of CO blobs (patches) within ODC stripes in supragranular layers have been reported for New World monkeys (14, 20), whereas CO blobs are located in the center of ODC stripes in macaques (6). In our staining, CO blobs were located in the center of ODC patches in peripheral V1, whereas they straddled ODC borders in central V1 (Fig. 4 *A* and *B* and Fig. S2). Furthermore, we found that the alignment of CO blobs tends to correspond with that of ODC patches for the ipsilateral eye in the portion of V1 that is representing peripheral vision (peripheral V1) in both hemispheres, suggesting that geniculate layers for the ipsilateral eye selectively project into, or beneath, CO blobs and the contralateral eye projects to interblobs in the peripheral V1 of owl monkeys.

In macaques, high levels of IEG expression were observed in "border strips" along the margins of activated ODC stripes after a brief (1- to 3-h) period of MI, but not after longer periods (16). We therefore tested the effects of short-term MI in owl monkeys. In 1-h MI cases, intense expression of IEG was detected along the borders of ODCs in layer 4 (4C) (Fig. 4*C*), suggesting that border strips are a widespread feature of ODCs in primates.

Discussion

Widespread Existence of ODC Revives Debate. The IEG expression patterns provided clear evidence for the existence of ODCs in all five owl monkeys examined. The unique features of ODC in owl monkeys are summarized in Fig. 5. As previously shown in macaque monkeys (16), higher levels of IEG expression occurred along the margins of ODCs in layer 4 (4C) only after short periods (1 h) of MI. We hypothesize that neurons along the margins of the ODC (border strip) are hyperactive owing to reduced inhibition from the inactivated ODC, but the misbalance is corrected over a recovery period owing to homeostatic mechanisms (discussed further in *SI Discussion*) (Fig. S3). The functions in vision of ODCs are presently unknown, and they are sometimes considered as the outcomes of developmental mechanisms without major implications for visual functions (6, 21). This

Fig. 4. (*A* and *B*) Examination of spatial relationship between CO blobs and OD domains in the tangential ipsilateral V1 sections to the blocked eye in owl monkey 11-04. Images for CO staining (*Top*) and ISH for *c-Fos* (*Middle*) are aligned exactly the same way guided by radial blood vessels. (*Bottom*) CO blobs are drawn by red over the image for *c-Fos*. *Insets* are magnification of the window in the same panel. In peripheral V1 (*A*), both CO blobs and ipsilateral OD domains line up in the corresponding way (arrows). In the central V1, no spatial correlation was observed between them (*B*). (Scale bar, 1 mm.) (*C*) An owl monkey case (ID 09-46) subjected to MI for 1 h. A tangential V1 section (1,050 μm from the pial surface; layer 4, ipsilateral to the blocked eye) was stained for *c-Fos* mRNA. (*Inset*) The magnification of the rectangle area. BS, border strip. (Scale bar, 1 mm.)

NEUROSCIENCE

Fig. 5. Schematic illustrations of V1 organization in owl monkeys revealed in this study. In peripheral V1, the ODC pattern is patchy surrounding MS, and CO blobs tend to colocalize OD patches for the ipsilateral eye, whereas the ODC pattern is stripes and does not have a spatial relationship with CO blobs in central V1. These patterns may continue into V2. OD domains are sometimes bridged in layer 4 (4C). There are BSs at the border of ODCs in layer 4 (4C).

idea was especially promoted by the capricious expression of ODCs in New World monkeys (7, 11), despite their capabilities of stereopsis (22). We suppose, however, that ODCs were not revealed in some of those monkeys owing to the low sensitivity of the CO method, and if cortex is examined for IEG expression instead, distinct representations of ODCs may be revealed. We consider that ODCs are a more common feature of V1 than formerly estimated, which suggests a reconsideration of the possible functional involvements of ODCs in vision. The variability in the details of the expression of ODCs across primate species offers an opportunity for productive modeling of the formation of ODCs and the computations of visual processing. Further investigation of IEG expression may reveal further differences and similarities of ODCs across primates and other nonprimate taxa. Studies in tree shrews would be especially interesting because it has been suggested previously that their ocular dominance domains are aligned in layers, rather than columns, in V1 (23, 24).

Technical Considerations. ODCs in V1 were first revealed in cats and macaques in electrophysiological recording studies (1). Later, the organization and presence of ODCs were more clearly identified using histological techniques, including transneuronal tracer injections and CO staining (2, 19). In the late 1980s, the uptake of radio-labeled 2-deoxy-D-glucose was measured to map neuronal activity differences in deprived and nondeprived ODCs (25). More recently, researchers used live imaging techniques, such as functional MRI and intrinsic signal optical imaging, to reveal cortical maps, which not only showed ODCs but also revealed spatial relationships with other functional features of V1 such as orientation columns (14, 26).

All of these techniques have pros and cons, such as having results restricted to a particular layer and having low spatial resolution. A demonstration of ODCs with IEG expression after MI was first introduced in macaques by Chaudhuri et al. (27) and was followed by its use in other studies (28). Other than in macaques, this procedure has also been applied in marmosets and cats (13, 29, 30). Those studies showed that IEG expression can imitate CO staining, but they did not use IEG expression to thoroughly study the representations of ODCs. We have noticed that the activity-dependent changes in IEG expression are capable of revealing functional compartments that have not been revealed by CO (16). In addition, at least in our preparations, ISH has a better signal/noise ratio than the immunohistochemistry, which has been commonly used to study IEG expression. Therefore, we believe that examination of IEG mRNA is the most sensitive of currently available methods of revealing ODCs.

Horton et al. (28) have previously reported that expected immunoreactivity of Zif268 ocular patterns occasionally reverse

after MI (i.e., in macaques, its expression is low in active ODCs and high in inactivated ODCs). In fact, this reversal in *Zif268* mRNA expression was observed in layer 4 (4C) of V1 in macaques in our previous study as well (16). Judging from the pattern observed in the MS of peripheral V1, this reversal did not occur in owl monkeys in our study, where *Zif268* mRNA expression was high in the ipsilateral and low in the contralateral MS. Therefore, IEG expression was high in open eye domains and low in closed eye domains in the owl monkeys of the present study.

Co-Occurrence of CO Blobs and ODCs in V1. As previously suggested for owl monkeys, squirrel monkeys, and galagos (15, 20, 30), there were no consistent topographical relationships between CO blobs and ODCs in the portion of V1 representing the central visual field in owl monkeys. However, the locations of CO blobs coincided with OD patches in the peripheral V1. The difference between representations of central and peripheral visual fields is consistent with the predictions of a theoretical model. Previous computer simulations have demonstrated that when the correlation in activity strength between the left- and right-eye inputs is low, the OD pattern becomes patchy for the less dominant eye, whereas when it is high, nearly equal ODC stripes are formed for both eyes (31). Furthermore, it has also been suggested that only when the correlation strength is low blobs tend to be located in the middle of ODCs (32). Balanced input from the left and right eyes and highly correlated interocular activity patterns, which are present for the central visual field, may result in the formation of ODC stripes with uniform band widths and the deviation of CO blob locations from the middle of ODC stripes. In contrast, the dominance of contralateral-eye inputs, and hence low interocular correlation that is seen in the representation of the peripheral visual field, may lead to the formation of ipsilateral-eye patches that coincide with CO blobs.

Ocular Dominance Domains in V2. Although the continuous ODC pattern crossing the V1/V2 border was only observed in one out of five owl monkeys examined in this study, this pattern might be common in this species. In three owl monkeys, the survival time after MI was shorter than 3 h, and this may not be enough to induce clear gene expression changes in V2: In those cases, OD pattern was hardly observed outside layer 4 (4C), even in V1. In the other case of 24-h MI (ID 11-04, Fig. 1), although faint, ODC-like stripes were also seen in V2 besides the CO thick/thin stripes (Fig. 4*B*). Therefore, MI longer than 24 h may constantly induce IEG expression that represents continuous OD stripes into V2 in owl monkeys.

In this regard, the observation that ODC stripes did not intersect the V1/V2 border at right angles in owl monkeys may be important. In most physical pattern formation theories, such as Rayleigh–Bénard convection and domain structures in magnetic thin films, stripe patterns intersect the free boundary at right angles, as do ODCs at the V1/V2 border in macaques and humans (19, 33). If ODC pattern formation follows these physical theories, the intersection of ODC stripes with the V1/V2 borders at oblique angles in owl monkeys implies that the pattern does not terminate at that border, that is, the ODC pattern continues from V1 into V2.

Indeed, it has been known that ODC pattern continues from area 17 (V1) to area 18 (V2) in cats (34). Although the LGN projects only sparsely to extrastriate visual areas (35), area 18 receives exclusive inputs from Y cells in the LGN, whereas area 17 receives both X and Y inputs from the LGN in cats (36). It would be interesting to examine details of geniculocortical connectivity in owl monkeys.

Bridged "Cortical Column" in Layer 4 (4C). Our data suggested that ocular segregation is rather coarse in the recipient layer 4 and becomes fractionated when layer 4 projects into upper layers, then

this fine pattern is maintained when the upper layers project into the infragranular layers (Fig. 5). This is a case of "cortical columns" that occasionally turn their property into the opposite direction when neurons project from layer 4 (4C) to layers 2/3. This sort of property shift across layers has also been reported for orientation tuning (37). Regarding terminology, the term ODC may not be adequate for describing the ocular dominance representation in owl monkeys. Mountcastle proposed, and Hubel supported, the concept that sensory cortices are composed of functional columns straightly coursing through the cortex from the pia to the white matter (38, 39). However, the model based on this concept seems too simplified to describe complicated cortical networks. In fact, most cortical modules are not exact "columns" throughout all layers (40). For example, barrels in the rodent primary somatosensory area (S1) are only observed in layer 4 (41), and islands in the entorhinal cortex are limited to superficial layers (42). Here, we add a different kind of "cortical column" to the literature. The variability in the width of OD domains in layer 4 (4C) of owl monkeys resembles the OD pattern reported in layer 4 (4C) of squirrel monkeys (11), and the fine OD pattern with constant width in supragranular layers is rather similar to the pattern in the macaque (19). In consideration of the report that OD domains are arranged into layers in tree shrews (23, 24), the owl monkey pattern may represent an intermediate between the tree shrew OD layer pattern and OD column pattern in macaques and humans.

Through electrophysiological recordings, Livingstone concluded that most of the neurons in layer 4 (4C) of owl monkeys are highly monocular, but their distribution may be a salt-and-pepper pattern in squirrel monkey V1 (7). This is also possible in owl monkeys, that is, although the distribution of left and right eye dominant neurons is roughly segregated, they may be intermixed in the same portion of layer 4 (4C), and when they project into upper layers this segregation becomes more distinct.

Materials and Methods

Animals and Sample Preparation. Five owl monkeys (*Aotus trivirgatus*, 1,000–1,200 g, either sex, adult) were given monocular injections of TTX. Under ketamine (10–20 mg/kg) and isoflurane (1%) anesthesia, 5 μL (1 mM) of TTX was slowly injected into the vitreous cavity of the left eye through a Hamilton syringe fitted with a glass pipette tip. After TTX placement, the owl moneys were brought back to their home cages, where they were recovered from anesthesia and allowed to move freely for 24 h (two cases), 3 h (one case), or 1 h (two cases). Because owl monkeys are nocturnal, their days and nights were reversed in their home cages in the animal facility; therefore, they were treated during nighttime conditions. Although previous researchers provided dark adaptation and photo-stimulation to induce IEG expression in the visual cortex after MI (13), those treatments were not needed in our preparation to detect sufficient IEG signals. After each owl monkey's specific recovery time, it was anesthetized again with ketamine, given an overdose of pentobarbital, and perfused intracardially with buffered saline followed by 2–4% paraformaldehyde in 0.1 M phosphate buffer (PB) by volume. The brain was removed from the skull and the visual cortices were flattened. The tissue was cryoprotected in 30% sucrose/PB at 4 °C for an additional one or two nights. The flattened brains were then frozen and cut into sections tangentially to the pial surface on a sliding microtome at a thickness of 30–40 μm. Some tissue was cut into coronal sections at a thickness of 40 μm. The tissue sections were maintained in a cryoprotectant solution (30% glycerol, 30% ethylene glycol, and 40% 0.1 M PBS) at −20 °C.

The protocols used in this study were approved by the Animal Research Committee of Animal Care and Use Committee at Vanderbilt University. They are in accordance with the animal care guidelines of the National Institutes of Health.

Histology. For colorimetric ISH, digoxigenin (DIG)-labeled antisense and sense riboprobes were prepared using a DIG-dUTP labeling kit (Roche Diagnostics). We used riboprobes for *Zif268* and *c-Fos* as in a previous study (16). The sense probes did not detect signals stronger than the background signal. The sequences were from macaques, and the exact sequences of IEGs in owl monkeys are not known. Nevertheless, we were able to detect sufficient ISH signals with these probes in owl monkey tissue, most likely because the sequences of genes of owl monkeys are highly homologous (more than 95%) to those of macaques (43). ISH was carried out as described previously (16, 43).

For architectonically identifying V1 and its laminar structure, one set of brain sections was processed for CO enzymatic activity (44). Free-floating sections were immersed into 10% sucrose/PBS (pH 7.4). Sections were then reacted with 0.50 mg/mL cytochrome C type III (Calbiochem), 0.25 mg/mL 3′, 3-diaminobenzidine (Sigma–Aldrich), and 0.37 mg/mL catalase (Sigma–Aldrich) in 10% sucrose/PBS at 37 °C for 6–12 h.

Data Analysis. Images of the ISH sections were captured with a Nikon Eclipse E800M microscope using a high-density CCD color digital camera, DXM1200F (Nikon). The images were edited and the brightness and contrast were enhanced using Photoshop CS3 Extended (Adobe Systems). To superimpose and compare staining patterns of serial sections, distortions and shrinkage of sections were digitally corrected. Because tangential sections sometimes contained different layers owing to incomplete flattening, some figures were made by mosaic from sections of different level.

To quantify intensity of CO staining and IEG mRNA expression, gray levels of ROI were measured and converted into ROD by the equation

$$ROD = \log_{10} \left(\text{observed gray level}/255 \right).$$

Background ROD was taken in layer 1 or white matter and subtracted from the original ROD. ROIs were chosen in DC and PC separately (Fig. 3), and the significance of expression changes by MI was examined in six sections from three hemispheres of two individuals with paired Student *t* test. *P* < 0.05 was considered a significant difference. The mean areas of ROI and their SE were 18.6 ± 7.3 mm² and 12.9 ± 4.3 mm² per section for DC and PC, respectively.

1. Hubel DH, Wiesel TN (1968) Receptive fields and functional architecture of monkey striate cortex. *J Physiol* 195(1):215–243.
2. LeVay S, Connolly M, Houde J, Van Essen DC (1985) The complete pattern of ocular dominance stripes in the striate cortex and visual field of the macaque monkey. *J Neurosci* 5(2):486–501.
3. Hubel DH, Wiesel TN (1972) Laminar and columnar distribution of geniculo-cortical fibers in the macaque monkey. *J Comp Neurol* 146(4):421–450.
4. Rosa MG, Gattass R, Fiorani Júnior M (1988) Complete pattern of ocular dominance stripes in V1 of a New World monkey, Cebus apella. *Exp Brain Res* 72(3):645–648.
5. Florence SL, Conley M, Casagrande VA (1986) Ocular dominance columns and retinal projections in New World spider monkeys (Ateles ater). *J Comp Neurol* 243(2):234–248.
6. Horton JC, Adams DL (2005) The cortical column: A structure without a function. *Philos Trans R Soc Lond B Biol Sci* 360(1456):837–862.
7. Livingstone MS (1996) Ocular dominance columns in New World monkeys. *J Neurosci* 16(6):2086–2096.
8. Kaas JH, Lin CS, Casagrande VA (1976) The relay of ipsilateral and contralateral retinal input from the lateral geniculate nucleus to striate cortex in the owl monkey: A transneuronal transport study. *Brain Res* 106(2):371–378.
9. Rowe MH, Benevento LA, Rezak M (1978) Some observations on the patterns of segregated geniculate inputs to the visual cortex in New World primates: An autoradiographic study. *Brain Res* 159(2):371–378.
10. Spatz WB (1989) Loss of ocular dominance columns with maturity in the monkey, Callithrix jacchus. *Brain Res* 488(1-2):376–380.
11. Adams DL, Horton JC (2003) Capricious expression of cortical columns in the primate brain. *Nat Neurosci* 6(2):113–114.
12. Fonta C, Chappert C, Imbert M (2000) Effect of monocular deprivation on NMDAR1 immunostaining in ocular dominance columns of the marmoset Callithrix jacchus. *Vis Neurosci* 17(3):345–352.
13. Markstahler U, Bach M, Spatz WB (1998) Transient molecular visualization of ocular dominance columns (ODCs) in normal adult marmosets despite the desegregated termination of the retino-geniculo-cortical pathways. *J Comp Neurol* 393(1):118–134.
14. Kaskan PM, Lu HD, Dillenburger BC, Roe AW, Kaas JH (2007) Intrinsic-signal optical imaging reveals cryptic ocular dominance columns in primary visual cortex of New World owl monkeys. *Front Neurosci* 1(1):67–75.
15. Xu X, Bosking WH, White LE, Fitzpatrick D, Casagrande VA (2005) Functional organization of visual cortex in the prosimian bush baby revealed by optical imaging of intrinsic signals. *J Neurophysiol* 94(4):2748–2762.

NEUROSCIENCE

16. Takahata T, Higo N, Kaas JH, Yamamori T (2009) Expression of immediate-early genes reveals functional compartments within ocular dominance columns after brief monocular inactivation. *Proc Natl Acad Sci USA* 106(29):12151–12155.

17. Zangenehpour S, Chaudhuri A (2002) Differential induction and decay curves of c-fos and zif268 revealed through dual activity maps. *Brain Res Mol Brain Res* 109(1-2): 221–225.

18. Hässler R (1967) *Evolution of the Forebrain*, eds Hassler R, Stephan H (Thieme, Stuttgart), pp 419–434.

19. Horton JC, Hocking DR (1998) Monocular core zones and binocular border strips in primate striate cortex revealed by the contrasting effects of enucleation, eyelid suture, and retinal laser lesions on cytochrome oxidase activity. *J Neurosci* 18(14): 5433–5455.

20. Horton JC, Hocking DR (1996) Anatomical demonstration of ocular dominance columns in striate cortex of the squirrel monkey. *J Neurosci* 16(17):5510–5522.

21. Purves D, Riddle DR, LaMantia AS (1992) Iterated patterns of brain circuitry (or how the cortex gets its spots). *Trends Neurosci* 15(10):362–368.

22. Livingstone MS, Nori S, Freeman DC, Hubel DH (1995) Stereopsis and binocularity in the squirrel monkey. *Vision Res* 35(3):345–354.

23. Hubel DH (1975) An autoradiographic study of the retino-cortical projections in the tree shrew (Tupaia glis). *Brain Res* 96(1):41–50.

24. Casagrande VA, Harting JK (1975) Transneuronal transport of tritiated fucose and proline in the visual pathways of tree shrew Tupaia glis. *Brain Res* 96(2):367–372.

25. Tootell RB, Hamilton SL, Silverman MS, Switkes E (1988) Functional anatomy of macaque striate cortex. I. Ocular dominance, binocular interactions, and baseline conditions. *J Neurosci* 8(5):1500–1530.

26. Lu HD, Roe AW (2008) Functional organization of color domains in V1 and V2 of macaque monkey revealed by optical imaging. *Cereb Cortex* 18(3):516–533.

27. Chaudhuri A, Matsubara JA, Cynader MS (1995) Neuronal activity in primate visual cortex assessed by immunostaining for the transcription factor Zif268. *Vis Neurosci* 12(1):35–50.

28. Horton JC, Hocking DR, Adams DL (2000) Rapid identification of ocular dominance columns in macaques using cytochrome oxidase, Zif268, and dark-field microscopy. *Vis Neurosci* 17(4):495–508.

29. Van Der Gucht E, Vandenbussche E, Orban GA, Vandesande F, Arckens L (2000) A new cat Fos antibody to localize the immediate early gene c-fos in mammalian visual cortex after sensory stimulation. *J Histochem Cytochem* 48(5):671–684.

30. Nakagami Y, Watakabe A, Yamamori T (2013) Monocular inhibition reveals temporal and spatial changes in gene expression in the primary visual cortex of marmoset. *Front Neural Circuits* 7:43.

31. Tanaka S (1991) Theory of ocular dominance column formation. Mathematical basis and computer simulation. *Biol Cybern* 64(4):263–272.

32. Nakagama H, Tanaka S (2004) Self-organization model of cytochrome oxidase blobs and ocular dominance columns in the primary visual cortex. *Cereb Cortex* 14(4): 376–386.

33. Adams DL, Sincich LC, Horton JC (2007) Complete pattern of ocular dominance columns in human primary visual cortex. *J Neurosci* 27(39):10391–10403.

34. Kaschube M, et al. (2003) The pattern of ocular dominance columns in cat primary visual cortex: Intra- and interindividual variability of column spacing and its dependence on genetic background. *Eur J Neurosci* 18(12):3251–3266.

35. Stepniewska I, Qi HX, Kaas JH (1999) Do superior colliculus projection zones in the inferior pulvinar project to MT in primates? *Eur J Neurosci* 11(2):469–480.

36. Freund TF, Martin KA, Whitteridge D (1985) Innervation of cat visual areas 17 and 18 by physiologically identified X- and Y- type thalamic afferents. I. Arborization patterns and quantitative distribution of postsynaptic elements. *J Comp Neurol* 242(2): 263–274.

37. Bauer R, Dow BM, Vautin RG (1980) Laminar distribution of preferred orientations in foveal striate cortex of the monkey. *Exp Brain Res* 41(1):54–60.

38. Mountcastle VB (1997) The columnar organization of the neocortex. *Brain* 120(Pt 4): 701–722.

39. Hubel DH, Wiesel TN (1977) Ferrier lecture. Functional architecture of macaque monkey visual cortex. *Proc R Soc Lond B Biol Sci* 198(1130):1–59.

40. Rockland KS (2010) Five points on columns. *Front Neuroanat* 4:22.

41. Woolsey TA, Welker C, Schwartz RH (1975) Comparative anatomical studies of the SmL face cortex with special reference to the occurrence of "barrels" in layer IV. *J Comp Neurol* 164(1):79–94.

42. Ichinohe N, Rockland KS (2004) Region specific micromodularity in the uppermost layers in primate cerebral cortex. *Cereb Cortex* 14(11):1173–1184.

43. Takahata T, Shukla R, Yamamori T, Kaas JH (2012) Differential expression patterns of striate cortex-enriched genes among Old World, New World, and prosimian primates. *Cereb Cortex* 22(10):2313–2321.

44. Wong-Riley M (1979) Changes in the visual system of monocularly sutured or enucleated cats demonstrable with cytochrome oxidase histochemistry. *Brain Res* 171(1): 11–28.